Organization of FtsZ Filaments in the Bacterial Division Ring Measured from Polarized Fluorescence Microscopy: Supplementary Material

Fangwei Si[1], Kimberly Busiek[2], William Margolin[2] and Sean X. Sun[1]
[1]*Department of Mechanical Engineering, Physical Sciences in Oncology Center, Whitaker Institute of Biomedical Engineering, Johns Hopkins University*
[2]*Department of Molecular Biology and Genetics, University of Texas Medical School, Houston TX.*

1 Materials and Methods

1.1 Protein purification and polymerization *in vitro*

To purify FtsZ and its fluorescently tagged derivatives, strains expressing each protein were grown from overnight cultures at a 1:100 dilution in 1.5-4.5 liters of Luria-Bertani (LB) broth supplemented with appropriate antibiotics (tetracycline, 5μg/ml; ampicillin, 100μg/ml). Cultures were grown at 37°C and induced during logarithmic phase using a final concentration of 1mM IPTG. Cells were collected after 2-5 hours by centrifugation at 10,000 X g. Pellets were resuspended using 40 ml lysis buffer (50mM Tris pH 8.0, 300mM NaCl, 10mM $MgCl_2$, 1mM EDTA) per liter of cells. Resuspended cells were incubated with lysozyme (4 mg/ml), phenylmethylsulfonyl fluoride (PMSF; 1mM), and beta-mercaptoethanol (0.1%) for one hour on ice. Cells were lysed using 10 cycles of sonication (50% duty cycle, output control 5, 30 seconds per cycle) and centrifuged at 10-12,000 X g. The resulting crude extract was brought to a final concentration of 35% $(NH_4)_2SO_4$, incubated on ice for 15 minutes, and centrifuged at 10,000 X g to reduce the amount of contaminating protein.

Following the ammonium sulfate cut, the pellet was homogenized in 25mM piperazine-N, N-bis[2-ethanesulfonicacid] (PIPES) pH 6.5 and centrifuged at 10,000 X g. The supernatant was brought to a final concentration of 1M sodium glutamate, 10mM MgSO4, and 1mM guanosine triphosphate (GTP) and incubated at 37°C for 30 minutes to promote polymerization. Polymerized protein was pelleted by centrifugation at 12,000 X g, resuspended in PIPES pH 7.4 buffer, and incubated on ice for 1 hour to depolymerize the protein. The resuspended pellet was centrifuged at 10,000 X g and the supernatant containing the depolymerized protein was stored at -80°C. The final concentration of each protein preparation was measured using the Bradford assay (native FtsZ, 3.2mg/ml; FtsZ1-338-YFP-FtsZ339-383 (referred throughout as FtsZ-YFP for simplicity), 0.3mg/mL; FtsZ-GFP, 0.1mg/ml; GFP-FtsZ, 1.4mg/ml). The final concentrations of each protein preparation was measured using the Bradford assay (native FtsZ, 3.2mg/ml; FtsZ-YFP, 0.3mg/ml; FtsZ-GFP, 0.1mg/ml; GFP-FtsZ, 1.4mg/ml; Caulobacter FtsZ-YFP 0.75-1mg/ml).

To polymerize bundles of FtsZ, wild-type FtsZ and FtsZ-YFP protein were diluted into 25mM PIPES with 1M sodium glutamate at pH 6.5 to final concentrations of 70 μg/ml and 200 μg/ml, respectively. Then, final concentrations of 1mM GTP and 10mM Magnesium sulfate were added.

On the other hand, to polymerize single filaments of FtsZ, final concentrations of wild-type FtsZ and FtsZ-YFP were both 20μg/ml. Final concentration of 1mM GTP was added, and that of Magnesium sulfate was reduced to 4mM.

For polymerization of C-terminal FtsZ-GFP bundles, final concentrations of wild-type FtsZ and FtsZ-YFP were 70μg/ml and 120μg/ml, respectively. For polymerization of C-terminal FtsZ-GFP protofilaments, final concentrations of wild-type FtsZ and FtsZ-YFP were both 20μg/ml. For polymerization of N-terminal GFP-FtsZ protofilaments, final concentrations of wild-type FtsZ and FtsZ-YFP were both 50μg/ml. Concentrations of GTP and magnesium sulfate are the same as FtsZ-YFP. To polymerize Caulobacter FtsZ-YFP, Caulobacter FtsZ-YFP were diluted into 25mM PIPES at pH 6.5 to a final concentration of 300μg/ml. Final concentrations of 1mM GTP and 10mM Magnesium sulfate were added.

1.2 Plasmid Construction

E. coli strains used for protein purification were constructed as follows: to fuse GFP to the amino-terminus of FtsZ (GFP-FtsZ), a plasmid-encoded copy of *E. coli* FtsZ was subcloned 3 to the GFP gene in plasmid pDSW207 using SacI and HindIII restriction sites. In this plasmid vector, the GFP gene is encoded upstream of the multiple cloning site. The resulting ApR plasmid was transformed into *E. coli* XL1-Blue, yielding strain WM3775. A carboxy-terminal fusion of GFP to FtsZ (FtsZ-GFP) was made by amplifying FtsZ with a forward primer encoding a SacI restriction site and a reverse primer encoding both a PstI restriction site and a tetra-asparagine linker to promote flexibility between FtsZ and GFP. The insert was digested with SacI and PstI and ligated into plasmid pDSW208. The GFP gene is located downstream of the multiple cloning site in pDSW208, allowing carboxy-terminal fusions of the inserted gene to GFP. The resulting ApR pDSW208-FtsZ plasmid was transformed into XL1-Blue to create strain WM3776. To construct an FtsZ-YFP fusion that would produce an FtsZ protein with an internal YFP, the EYFP gene was PCR-amplified with primers 1201 (GTT CAG CAG CCA GTG ATG GAT CGC AGT AAA GGA GAA GAA CTT TTC ACT) and 1202 (CGG AGC CAT CCC ATG CTG CTG GTA TTT GTA TAG TTC ATC CAT GCC ATG). The sequences corresponding to FtsZ are underlined. The amplified product was then used as a mega-primer for the Quikchange mutagenesis kit, using pDSW208-FtsZ (no fusion to GFP) as a template, inserting the EYFP between amino acid residues 338 and 339 of FtsZ to make FtsZ1-338-YFP-FtsZ339-383 (FtsZ-YFP). This corresponds to the linker region between the polymerization domain (1-320) and the C-terminal tail (370-383) of FtsZ. The FtsZ-YFP fusion was cloned into pDSW208 and transformed into XLI-Blue to make strain WM3308. Native FtsZ was overproduced from strain WM971, which carries FtsZ downstream of the T7 promoter of expression vector pET11a; this strain was a gift from Harold Erickson.

1.3 Cell Synchronization

C-terminal FtsZ-GFP E. coli strain was cultured in M9 media with 0.2% acetate. In this minimal nutrient media, the doubling time of *E. coli* cells is elongated to 3 hours; the DNA copy number is always between 1N-2N [1]. To synchronize the cell cycle, DL-serine hydroxamate (SigmaAldrich, S4503) was added to a final concentration of 1 mg/ml, which stops cell cycle at a new round of DNA replication. Ongoing rounds of replication still progress to completion [1]. Then, serine hydroxamate was washed out after all ongoing DNA replications are completed. Cells resumed the cell cycle in good synchrony. Polarization microscopy was done within the first cell cycle after the

synchronization, and data from two time points before and after the formation of visible septum were analyzed and compared.

1.4 Z-linker Constructs

In their polarized fluorescence microscopy experiments, Kampmann et al. [2] created a fusion of Saccharomyces cerevisiae protein Nic96 to GFP that was functional in vivo and yielded a high amplitude in anisotropy readings. This construct, Nic96-GFP(-8/-5), is composed of Nic96 protein that is truncated at its C-terminal alpha helix by 8 amino acid residues and GFP that is truncated at its N-terminal alpha helix by 5 amino acid residues. The fusion of the two truncated proteins yields a single, rigid alpha helix at the fusion site RETYST/ELF, where RETYST are residues 826-831 of Nic96 and ELF are residues 6-8 of GFP. To create a more rigid linker between FtsZ and GFP, the Nic96-GFP linker region (RETYSTELF) was inserted between FtsZ and the remainder of GFP (residues 9-238) forming FtsZ-Nic96$_{\mathrm{linker-trunc}}$GFP. To make this construct, we first amplifed FtsZ with a forward primer encoding a SacI site and the N-terminus of ftsZ (#1430) and a reverse primer encoding the C-terminus of FtsZ, the linker region RETYSTELF, and residues 9 and 10 of GFP (#1733). In a separate reaction, we amplified *gfp* using a forward primer that also encoded the C-terminus of FtsZ, the linker region RETYSTELF, and residues 9 and 10 of GFP (#1732) and a reverse primer encoding the C-terminus of GFP and a PstI site (#1736). We then used combinatorial PCR to combine both PCR products using primers #1430 and #1736. The final PCR product was digested with SacI and PstI restriction enzymes and ligated into vectors pDSW208 and pDSW208-*flag*, which contains a flag sequence between EcoRI and SacI sites. pDSW208-ftsZ-nic96$_{\mathrm{linker-trunc}}$gfp and pDSW208-flag- ftsZ-nic96$_{\mathrm{linker-trunc}}$gfp were transformed into XL1-Blue cells yielding WM4363 and WM4364, respectively.

Similar to the approach used by Kampmann et al. [2], we truncated the C-terminal alpha helix of FtsZ by 4 amino acid residues and fused it directly to N-terminally truncated GFP to create $_{\mathrm{trunc}}$FtsZ-truncGFP. We made this construct by first amplifying truncated ftsZ (encoding residues 1-379) using a forward primer encoding a SacI site and the N-terminus of ftsZ (#1430) and a reverse primer encoding residues 374-379 of FtsZ and residues 6-11 of GFP (#1735). In a separate reaction, we amplified gfp (residues 6-238) using a forward primer encoding residues 374-379 of FtsZ and residues 6-11 of GFP (#1734) and a reverse primer encoding the C-terminus of GFP and a PstI site (#1736). We used combinatorial PCR to combine both PCR products using primers #1430 and #1736. The final PCR product was digested with SacI and PstI restriction enzymes and ligated into vectors pDSW208 and pDSW208-*flag*. pDSW208-$_{\mathrm{trunc}}$ftsZ-$_{\mathrm{trunc}}$gfp and pDSW208-flag-$_{\mathrm{trunc}}$ftsZ-$_{\mathrm{trunc}}$gfp were transformed into XL1-Blue cells yielding WM4365 and WM4366, respectively.

2 Supporting Text

2.1 Orientational distribution of fluorophore dipoles *in vitro*

As shown in Fig. S1, after filtering by the polarizer, the excitation light has an orientation parallel to the focal plane. Thus, neglecting phases, the incoming excitation electric vector is

$$\mathbf{E}_{in} = \sqrt{I_{in}}\mathbf{p} \tag{1}$$

where I_{in} is the intensity of the excitation light, and $\mathbf{p}$ is a unit vector in the direction of the electric vector.

After passage through the objective, some depolarization occurs and the excitation light is no longer fully polarized in the **p** direction. Taking into account this depolarizing effect, the excitation light after passing through the objective can be written as

$$\mathbf{E}_{in} = \sqrt{I_{in}}(I_p\mathbf{p} + I_q\mathbf{q} + I_r\mathbf{r}) \tag{2}$$

where **q** is a unit vector perpendicular to the polarization direction, **r** is a unit vector in the direction of propagation, and $I_{p,q,r}$ are the components of $\mathbf{E}_{excitation}$ in $(\mathbf{p}, \mathbf{q}, \mathbf{r})$ directions. In our experiment, **q** correspond to the Lab X -axis (shown in Fig. S1 in the supplemental material); **r** correspond to the Lab Y-axis and **p** is orthogonal to $(\mathbf{q}, \mathbf{r})$. The microscope objective we use has a numerical aperture of $NA = 1.45$. If we integrate over the electrical field in the focal plane, we have $I_p = 0.62$, $I_q = 0.08$ and $I_r = 0.30$ [3].

When interacting with the fluorophore *in vitro*, the incoming light is also the light exciting the fluorophore: $\mathbf{E}_{in} = \mathbf{E}_{excitation}$. Only the projection of excitation light on the orientation of fluorophore dipole is absorbed, and then emitted

$$\mathbf{E}_{emission} \propto (\mathbf{E}_{excitation} \cdot \mathbf{D})\mathbf{D} \tag{3}$$

where **D** is the fluorophore dipole vector [4]. This is because the rotational correlation time of fluorophores such GFP and YFP is significantly longer than their fluorescence lifetime [5, 6]. Also for GFP and YFP used in this study, the fluorphores' absorption and emission transition dipoles are mostly parallel [5, 7]. The emitted light is then filtered by the analyzer, and the analyzed light is collected by the camera. Taking into account depolarization effects of the emission through a high numerical aperture objective, the emitted fluorescence intensity collected by the camera is

$$\begin{aligned} I_{out} &\propto (\mathbf{E}_{out})^2 \propto I_{in}\left[K_p(\mathbf{E}_{emission}\cdot\mathbf{p})^2 + K_q(\mathbf{E}_{emission}\cdot\mathbf{q})^2 + K_r(\mathbf{E}_{emission}\cdot\mathbf{r})^2\right] \\ &\equiv I_{in} f(\mathbf{p}, \mathbf{q}, \mathbf{r}, \mathbf{D}) \end{aligned} \tag{4}$$

where $\mathbf{E}_{out}$ is the final electric vector reaching the camera, $K_{p,q,r}$ is the fraction of the component of $\mathbf{E}_{out}$ in the directions of $(\mathbf{p}, \mathbf{q}, \mathbf{r})$ [8]. Here, for an objective with $NA = 1.45$, we use $K_p = 0.377$, $K_q = 0.011$ and $K_r = 0.144$.

We also vary the polarizer direction with respect to the lab axis and compare the emission intensities when the polarization is parallel and perpendicular to **p**-axis. Therefore, the excitation field in the parallel direction is

$$\mathbf{E}_{in,||} = \sqrt{I_{in}}(I_p\mathbf{p} + I_q\mathbf{q} + I_r\mathbf{r}) \tag{5}$$

$$\begin{aligned} I_{||} &\propto I_{in}\left[K_p(\mathbf{E}_{out,||}\cdot\mathbf{p})^2 + K_q(\mathbf{E}_{out,||}\cdot\mathbf{q})^2 + K_r(\mathbf{E}_{out,||}\cdot\mathbf{r})^2\right] \\ &\equiv I_{in} f_{||}(\mathbf{p}, \mathbf{q}, \mathbf{r}, \mathbf{D}) \end{aligned} \tag{6}$$

and (note (I_p, I_q) have changed places)

$$\mathbf{E}_{in,=} = \sqrt{I_{in}}(I_q\mathbf{p} + I_p\mathbf{q} + I_r\mathbf{r}) \tag{7}$$

$$\begin{aligned} I_{=} &\propto I_{in}\left[K_q(\mathbf{E}_{out,=}\cdot\mathbf{p})^2 + K_p(\mathbf{E}_{out,=}\cdot\mathbf{q})^2 + K_r(\mathbf{E}_{out,=}\cdot\mathbf{r})^2\right] \\ &\equiv I_{in} f_{=}(\mathbf{p}, \mathbf{q}, \mathbf{r}, \mathbf{D}) \end{aligned} \tag{8}$$

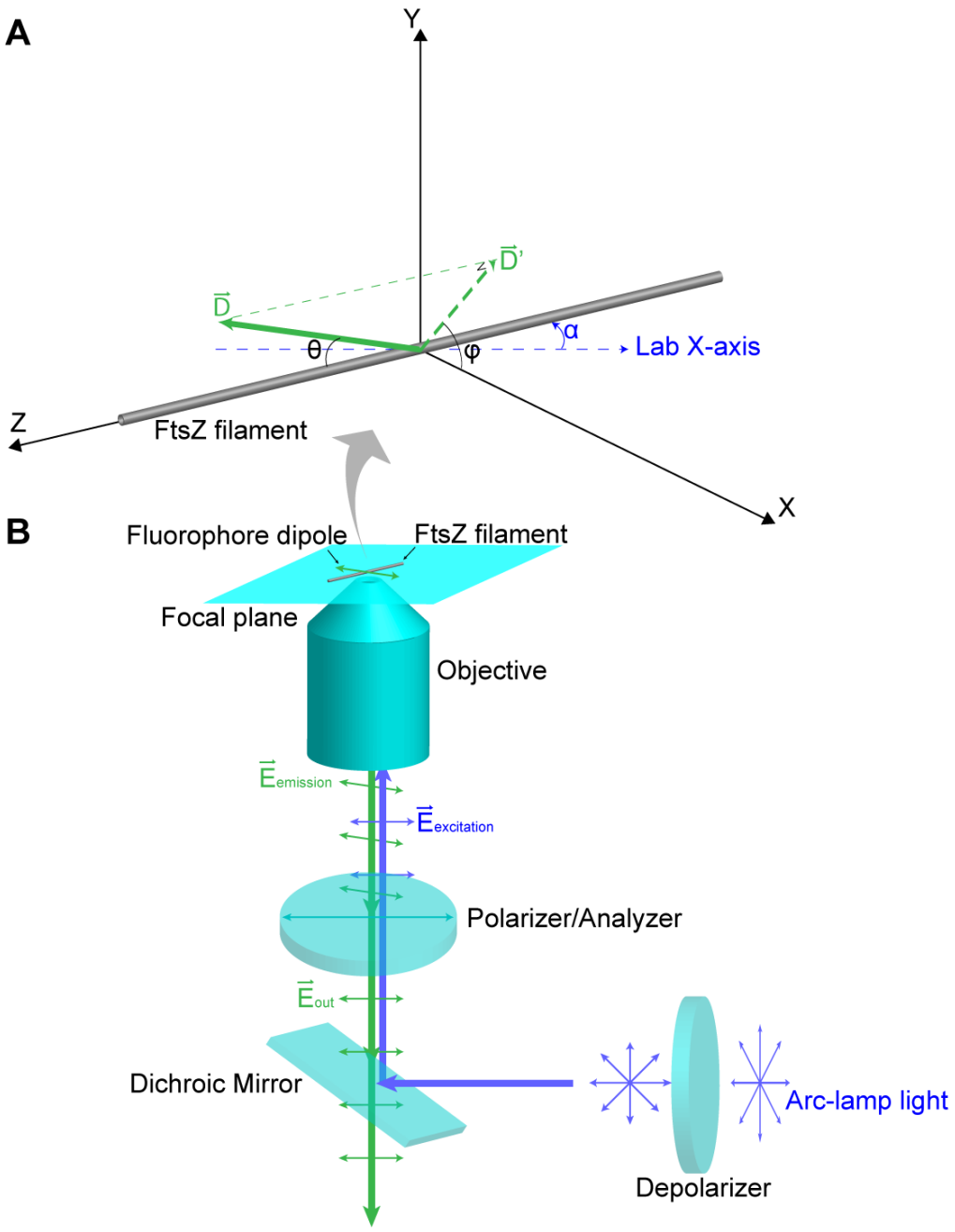

Fig. S 1: The microscopy setup showing the arrangement of the polarizers and the coordinate system describing the direction of the fluorophore attached to FtsZ filaments. (A) For protofilaments and bundles, we define the orientation of the fluorophore with respect to filament direction using angles θ and ϕ, where $\mathbf{D}$ is the fluorophore dipole vector and $\mathbf{D}'$ is its projection on the XY plane. (B) The microscopy setup using two polarizers. The sample is analyzed with respect to the polarization direction. The angle between the lab X-axis and the filament is defined by α. The polarization anisotropy is plotted as a function of the angle α. The same setup is used for *in vitro* and *in vivo* experiments.

where the || polarizer direction is along $\mathbf{p}$ and the = polarizer direction is along $\mathbf{q}$.

For small bundles of FtsZ *in vitro*, the fluorophore dipole is fluctuating rapidly on the time scale of the experiment. The probability distribution of the fluorophore dipole needs to be considered to quantitatively analyze the data. As shown in Fig. S1, we use two angles, θ and ϕ, to define $\mathbf{D}$. Therefore, the average collected fluorescence intensity is

$$\langle I_{||} \rangle \propto \langle I_{in} f_{||}(\mathbf{p}, \mathbf{q}, \mathbf{r}, \mathbf{D}) \rangle \propto I_{in} \int_0^{2\pi} \int_0^{\pi} f_{||}(\mathbf{p}, \mathbf{q}, \mathbf{r}, \mathbf{D}) \rho(\mathbf{D}) \sin\theta d\theta d\phi \tag{9}$$

and similarly for $\langle I_{=} \rangle$. The probability distribution $\rho(\mathbf{D})$ is the orientational distribution of the dipole, which we take as

$$\rho(\mathbf{D}) = p(\phi) p(\theta). \tag{10}$$

where

$$p(\phi) = p(\phi; a, \phi_0) = \frac{e^{a\cos(\phi-\phi_0)}}{\int_0^{2\pi} e^{a\cos(\phi-\phi_0)} d\phi} \tag{11}$$

$$p(\theta) = p(\theta; b, \theta_0) = \frac{e^{b\cos[2(\theta-\theta_0)]}}{\int_0^{\pi} e^{b\cos[2(\theta-\theta_0)]} \sin\theta d\theta} \tag{12}$$

Here a and b are parameters describing the widths of the angular distributions. ϕ_0 and θ_0 are the centers of the distributions, these orientations represent the most probable orientation of the fluorophore.

By collecting fluorescence data from randomly oriented FtsZ protofilaments, we can calculate the polarization anisotropy as

$$P(\alpha) = \frac{\langle I_{||} \rangle - \langle I_{=} \rangle}{\langle I_{||} \rangle + \langle I_{=} \rangle} = P(\alpha; a, b, \phi_0, \theta_0) \tag{13}$$

where α is the angle of the protofilament with respect to the lab X-axis (Fig. S1). This is experimentally measured. Therefore by fitting the experimental curve, we can obtain information about the orientational probability distribution of the fluorophore with respect to the filament.

Using nonlinear optimization in Matlab, we have determined the parameters for a, b, β_0 and ϕ_0 that best explain the experimental data. In Fig. S2, we see that for the *in vitro* FtsZ-YFP protofilaments, we can only obtain a good fit to the experimental data when $\theta_0 = 0^\circ$ and $\phi_0 = 0^\circ$. Thus, the most probable orientation of the fluorophore is parallel to the protofilament. However, the distributions are quite broad (relatively small a and b values), the probability of observing other fluorophore orientations are quite high. These results suggest that the fluorophore has an angular distribution roughly equal to the distribution shown in Fig. S2 around the protofilament direction.

The fitted results for FtsZ-YFP bundles show generally the same θ_0 and ϕ_0 values, but with narrower distribution widths (Fig. S2(B)). This is sensible since in a bundle, fluorophore fluctuations are presumably more constrained. PFM is able to measure this change in orientational distribution.

Results from GFP-FtsZ and FtsZ-GFP filaments are also examined using this approach. We find that θ_0 and ϕ_0 are all similar, indicating that the fluorophore generally is aligned with the filament direction. This alignment does not appear to depend on the position of fluorophore label, although the width of the distributions does show some variation.

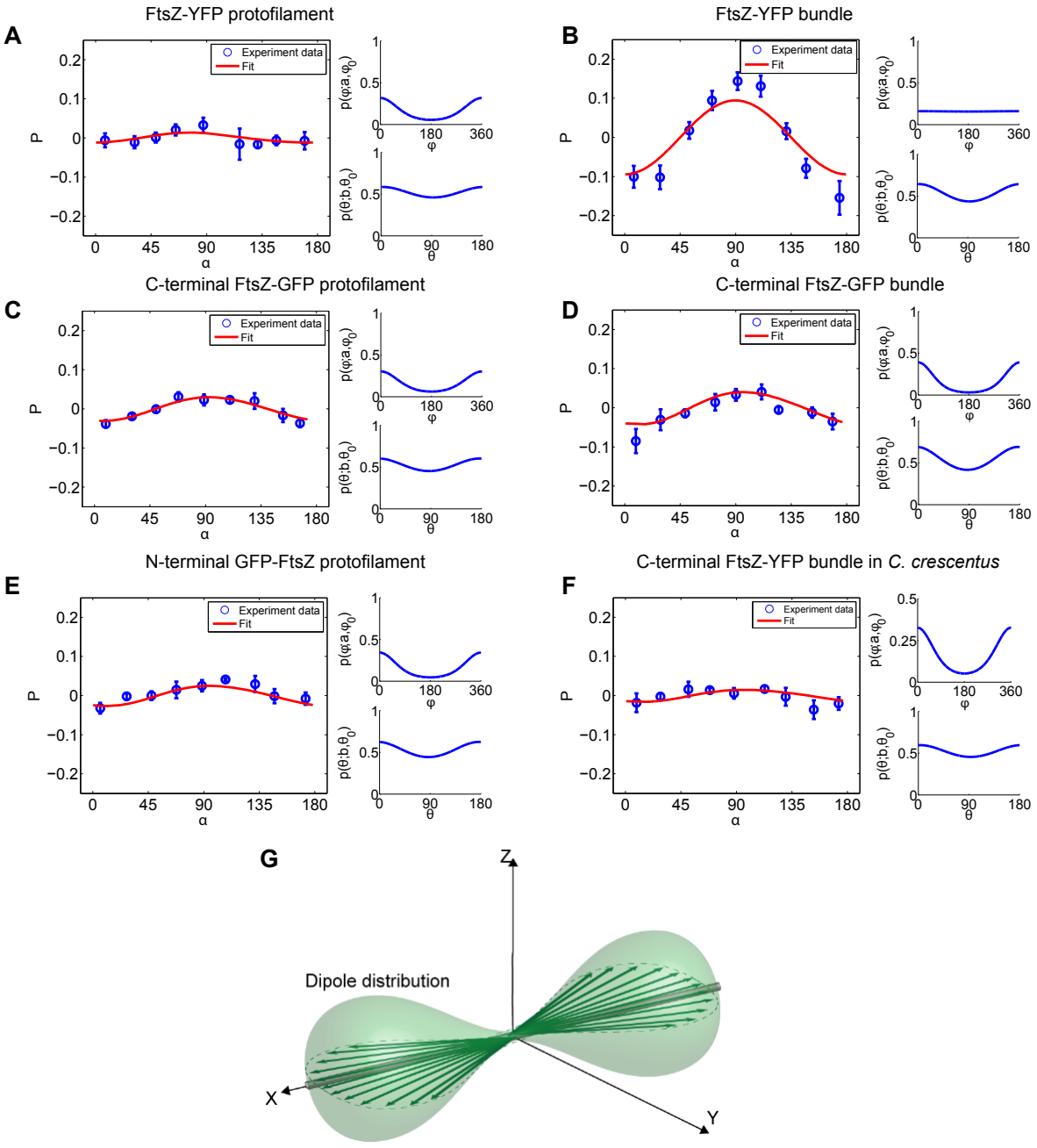

Fig. S 2: Calculation of orientational distribution of fluorophore dipole *in vitro*. The fitted fluorophore distributions for polarization data from (A) FtsZ-YFP protofilaments and (B) bundles, and (C) C-terminal FtsZ-GFP protofilaments, (D) C-terminal FtsZ-GFP bundles, (E) N-terminal GFP-FtsZ protofilaments, and (F) C-terminal FtsZ-YFP in *C. crescentus*. The best fit distributions for C-terminal FtsZ-YFP, FtsZ-GFP and N-terminal GFP-FtsZ protofilaments all show highest probability at $\theta_0 = \phi_0 = 0$, which is the orientation where the fluorophore dipole is parallel to the filament. (Note PFM is unable to decipher whether the dipole is parallel or antiparallel to the filament.) (G) A cartoon of the 3D orientational distribution of fluorophore dipoles around the FtsZ filament. There is some orientational disorder. The *average* dipole directions are along the filament.

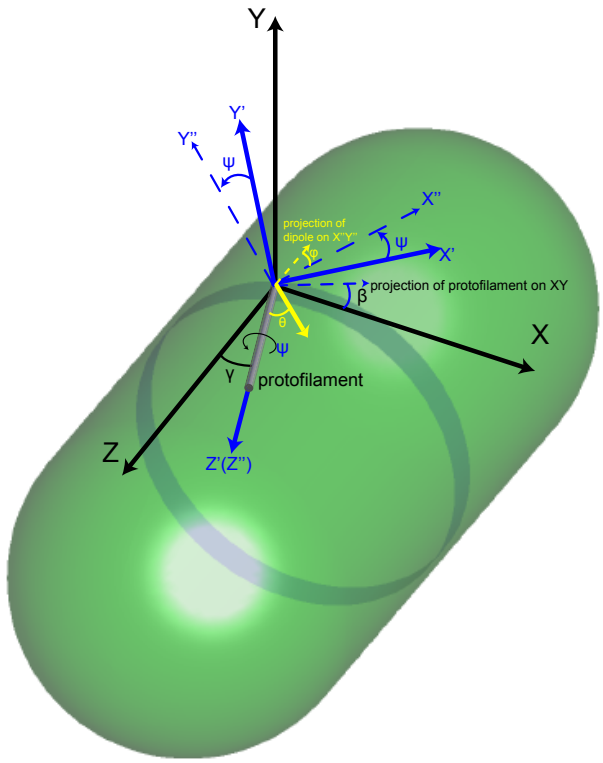

Fig. S 3: Coordinate system describing the orientation of the fluorophore dipole with respect to the protofilament in the local frame of the cell (X, Y, Z). In reality, filaments in the cell are not precisely aligned in the same direction. The protofilament orientation is described by an orientational distribution. The relationship between the fixed cell frame and the local frame of the fluctuating filament (X'', Y'', Z'') is given by the rotation matrix $\mathbf{R}$. The rotation procedure is given in the text.

2.1.1 Optical anisotropy of bacterial cell body and correction of PFM data

As common for many biomaterials, we found that the bacterial cell itself is optically anisotropic. For instance, the peptidoglycan layer, the cell membrane or other protein structures in the cell could be birefriengent, which will influence the results of polarized microscopy. If this is the case, depolarized light emitted within the cell body can become partly polarized. To examine this, we performed polarized microscopy on *E. coli* that only expresses freely diffusing GFP in the cytoplasm (Fig. S4). The freely rotating GFP molecules should only emit completely depolarized fluorescence. In our measurement, we also use a relatively long exposure time so that rotational diffusion should give isotropic fluorescence.

Our measurements show that fluorescent signals from diffusing GFP still shows some polarization anisotropy. The anisotropy is small (Fig. S4A). This result implies that the bacterial cell is optically anisotropic and converts the isotropic fluorescence emitted from freely diffusing GFP into partly polarized light. To quantitatively describe this intrinsic anisotropy, we can decompose the incoming and outgoing light into two components. One component is along the cell axis (Z in Fig S3) and the other component is along the circumferential direction (X). We use a parameter C which is the ratio of the circumferential component to the axial component to describe the amount of optical anisotropy:

$$\mathbf{E}_{excitation} = \mathbf{B}(\alpha) \cdot \mathbf{E}_{in} \tag{14}$$

where $\mathbf{B}$ is a transmission matrix that depends on the angle of the cell with respect to the incoming light $\mathbf{E}_{in}$.

$$\mathbf{B} = \begin{pmatrix} C\cos\alpha & 0 & C\sin\alpha \\ 0 & 1 & \\ -\sin\alpha & 0 & \cos\alpha \end{pmatrix} \tag{15}$$

Similarly, the light received by the photo detector is also a similar function of the emitted light.

$$\mathbf{E}_{out} = \mathbf{B}(\alpha) \cdot \mathbf{E}_{emission} \tag{16}$$

The fit shows $C = 0.984$, which means the circumferential component is roughly 2 percents smaller than the axial part. Similar measurements for free YFP in *C. crescentus* also shows polarization anisotropy, with $C = 0.975$ (Fig. S5).

With the quantitative result from the freely diffusing GFP, we then use this intrinsic anisotropy to correct the data for all *E. coli* strains with GFP or YFP fused with FtsZ in the Z-ring (Fig. S4 and S5). Here we assume the cellular optical anisotropy effects are equal for all different strains because of the same cell wall structure. After the correction, all polarization anisotropy plots show smaller amplitudes, which means the Z-ring is less anisotropic if the cellular optical anisotropy is considered (Fig. S4). However, *C. crescentus* FtsZ-YFP data shows a different maximum after correction (Fig. S5).

2.2 Orientational distribution of FtsZ-ring filaments in live cells

Having examined the orientation of the fluorophores *in vitro*, it is then possible to obtain estimates of the filament orientation *in vivo*. Since N- and C-terminal GFP and YFP tagged FtsZ all show similar polarization results both *in vitro* and *in vivo*, it is reasonable to conclude that in the live cell the fluorophore orientation on the FtsZ protofilaments are similar as *in vitro* situation. Using the orientational distributions of fluorophores with respect to protofilaments *in vitro*, we can then

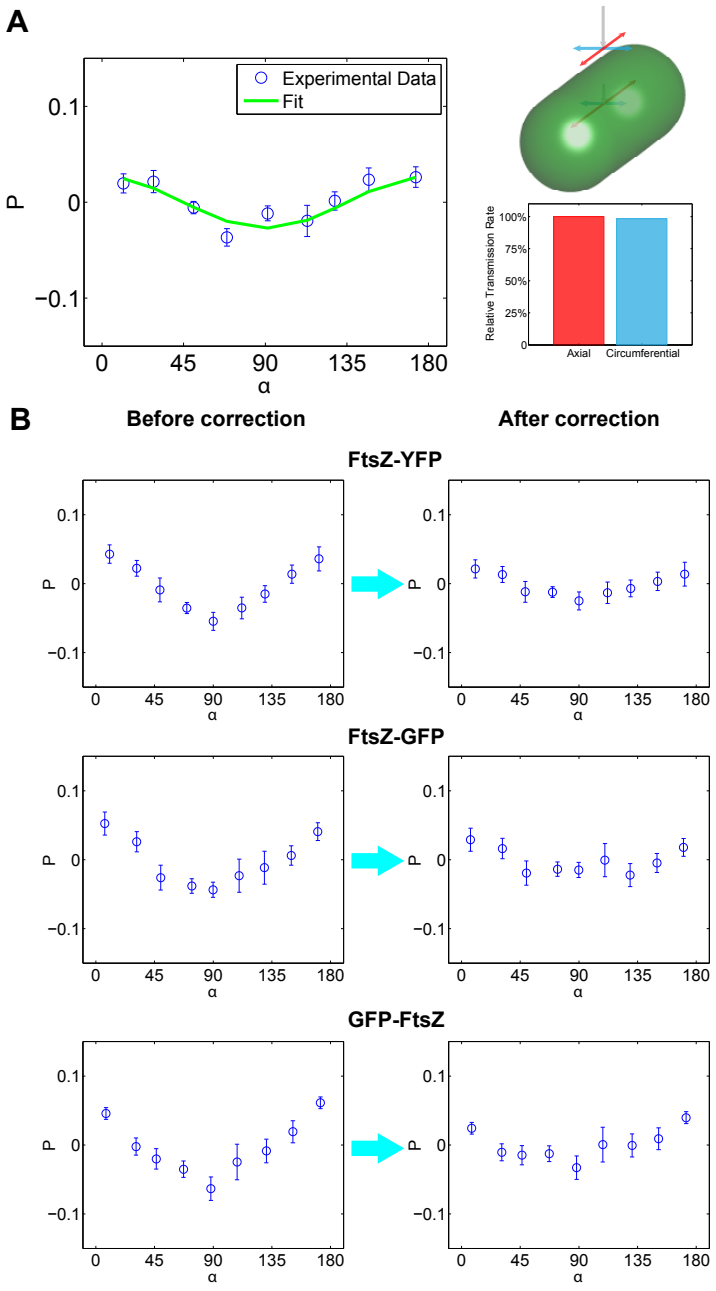

Fig. S 4: (A) Intrinsic polarization anisotropy in bacterial cells with freely diffusing GFP in *E. coli*. The angle α is the angle of the cell axis with respect to the lab X-axis. The intrinsic anisotropy could arise from birefringence of biomaterials such as the cell wall. (B) We can use the free GFP data as a calibration reference to correct anisotropy results from fluorophores attached to FtsZ. The correction accounts for anisotropic transmission of excitation and emitted light.

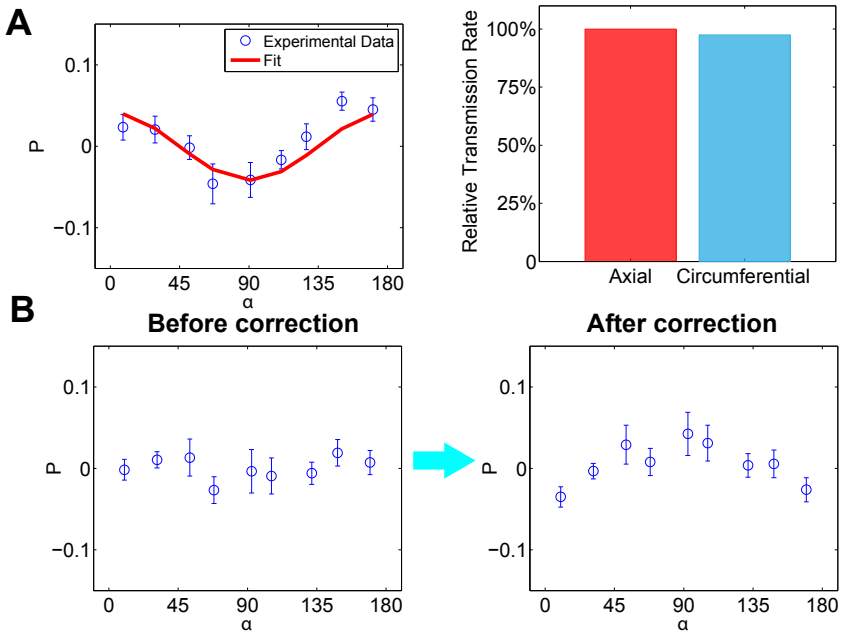

Fig. S 5: (A) Intrinsic polarization anisotropy in bacterial cells with freely diffusing YFP in *C. crescentus*. The intrinsic anisotropy could arise from birefringence of biomaterials such as the cell wall. (B) We can use the free YFP data as a calibration reference to correct anisotropy results from FtsZ-YFP.

infer the orientational distribution of FtsZ filaments *in vivo* by fitting the polarization data both from side view and cross-sectioned view. As shown in Fig. S3, we use two spatial angles β and γ to describe filament orientations in the lab frame. We explicitly consider two possibilities (Fig. S6), FtsZ filaments in the ring which are oriented in the cell-axis direction and in the cell circumference direction. α is the angle between the Z-ring and the lab X-axis. We use the data to obtain the best fit distributions in these two directions. We ask whether the data can be quantitatively explained by these orientations.

The direction of the fluorophore dipole in the local frame of the cell, $\mathbf{D}$, can be computed as (Fig. S6A)

$$\mathbf{D} = \mathbf{R} \cdot \mathbf{u}(\theta, \phi) \tag{17}$$

where $\mathbf{u}$ is the direction of the fluorophore dipole in the local frame with respect to the filament and $\mathbf{R}$ is a rotation from the filament frame to the local cell frame (Fig. S3). Since the orientation of the fluorophore is defined by angles θ and ϕ in the frame (X'', Y'', Z''), we first find (X', Y', Z') by rotating along the Y-axis by γ and then along the Z-axis by β. To go from (X', Y', Z') to (X'', Y'', Z''), we then rotate along Z' by angle ψ. Thus, the overall rotation from the lab frame (X, Y, Z) to (X'', Y'', Z'') is specified by three angles (β, γ, ψ). The rotation matrix is

$$\mathbf{R} = \begin{pmatrix} \cos\beta\cos\gamma\cos\psi - \sin\beta\sin\psi & -\cos\beta\cos\gamma\sin\psi - \sin\beta\cos\psi & \cos\beta\sin\gamma \\ \sin\beta\cos\gamma\cos\psi + \cos\beta\sin\gamma & -\sin\beta\cos\gamma\sin\psi + \cos\beta\cos\gamma & \sin\beta\sin\gamma \\ -\sin\gamma\cos\psi & \sin\gamma\sin\psi & \cos\gamma \end{pmatrix} \tag{18}$$

Note ψ has no direct bearing on the direction of the filament, it simply defines the fluorophore position with respect to the filament.

In the live cell fluorescence measurement, cytoplasmic FtsZ, which has an isotropic angular distribution, will contribute to the final signal. Therefore, the fluorophore angular distribution is a sum from the cytoplasmic component and the Z-ring component: $\Gamma = \Gamma_1 + \Gamma_2$. It was reported that 30-40% of FtsZ resides in the Z-ring[9, 10]. From our own data, we find that 40% of the labeled FtsZ is in the Z-ring. Within the cropped Z-ring image, FtsZ in the Z-ring is 70% of the total signal and the cytoplasmic FtsZ accounts for 30%. Therefore, the cytoplasmic angular distribution should be $\Gamma_2 = 0.3/8\pi^2$. The Z-ring FtsZ distribution, Γ_2, is described by the filament angular distributions in the local cell frame as $\Gamma_2 = 0.7 \times p(\beta)p(\gamma)p(\psi)$, where

$$p(\beta) = p(\beta; c, \beta_0) = \frac{e^{c\cos(\beta-\beta_0)}}{\int_0^{2\pi} e^{c\cos(\beta-\beta_0)} d\beta} \tag{19}$$

$$p(\gamma) = p(\gamma; d, \gamma_0) = \frac{e^{d\cos[2(\gamma-\gamma_0)]}}{\int_0^{\pi} e^{d\cos[2(\gamma-\gamma_0)]} \sin\gamma d\gamma} \tag{20}$$

$p(\psi)$ is also similarly defined. Given the filament angular distribution, the total measured fluorescence intensity is then

$$\langle I_{||} \rangle \propto I_{in} \int_0^{2\pi} \int_0^{\pi} \int_0^{2\pi} \int_0^{2\pi} \int_0^{\pi} f_{||}(\mathbf{p}, \mathbf{q}, \mathbf{r}, \mathbf{D}) \rho(\theta, \phi) \Gamma(\beta, \gamma, \psi) \sin\theta d\theta d\phi \sin\gamma d\psi d\beta d\gamma \tag{21}$$

where ρ is the fluorophore distribution with respect to the filament. ρ has been determined *in vitro* and we use the same distribution to compute the *in vivo* data.

Table 1: Best fit parameters for angular distributions in Eqs. (5) and (6) in the main text (Eqs. (11) and (12) in the SM), describing the orientation of the fluorophore with respect to the FtsZ filament *in vitro*.

In vitro orientation with respect to FtsZ	a (width of $p(\phi)$)	b (width of $p(\theta)$)	ϕ_0	θ_0
FtsZ-YFP	0.87	0.12	0°	0°
FtsZ-YFP Bundle	0.01	0.19	0°	0°
FtsZ-GFP	0.79	0.14	0°	0°
FtsZ-YFP Bundle	1.26	0.25	0°	0°
GFP-FtsZ	1.00	0.17	0°	0°
C. crescentus FtsZ-YFP	0.92	0.13	0°	0°

2.2.1 Fitting of orientational distribution of Z-ring laments in live cells

To examine the *in vivo* data, we look for *average* angular orientation β_0 and γ_0 that minimize the overall error between data and the theoretical curve. For each β_0 and γ_0, we optimize the other variables (c, d) to achieve minimum error. We use the data from the very top slice to avoid any geometrical effects. The results and fitted distributions are shown in Fig. S6 for FtsZ-YFP. We see that both average axial and average circumferential orientations can explain the data. However, these distributions are consistent with each other, since the fitted filament distributions are all quite broad. Both types of fits show significant axial and circumferential orientation for some filaments.

These quantitative data suggest an essentially disordered organization for FtsZ in *E. coli*, where large portions of the filaments are oriented in axial as well circumferential directions.

Similar results are obtained for C-terminal FtsZ-GFP (Fig. S7) and N-terminal GFP-FtsZ (Fig. S8). Indeed, it is possible to fit this data with other average orientations. But the fitted distributions all are very broad, showing significant disorganized arrangement. In Figs. S6, S7 and S8, we show representative FtsZ filament arrangements in the Z-ring based on the fitted distributions, the results from these strains are consistent with each other.

Table 2: Best fit parameters for angular distributions in Eqs. (11) and (12) in the main text (Eqs. (19) and (20) in the SM), describing the orientation of the FtsZ filaments in the Z-ring with respect to the cell axial and circumferential directions. We use two different average orientations: axial and circumferential. The fitted parameters indicate broad angular distributions and are consistent with each other. The pictorial representations of these distributions are shown in Figure 5 and Figure S6-S9

In vivo FtsZ orientation	c (width of $p(\beta)$)	d (width of $p(\gamma)$)	β_0	γ_0
E. coli FtsZ-YFP axial	4.98	1.10	0°	0°
E. coli FtsZ-YFP circumferential	5.00	0.00	0°	0°
E. coli FtsZ-GFP axial	5.00	0.11	0°	0°
E. coli FtsZ-GFP circumferential	5.00	0.06	0°	0°
E. coli GFP-FtsZ axial	5.00	0.28	0°	0°
E. coli GFP-FtsZ circumferential	5.00	0.00	0°	0°
C. crescentus FtsZ-YFP axial	5.00	0.00	0°	0°
C. crescentus FtsZ-YFP circumferential	0.00	4.93	0°	0°

2.3 Axial versus circumferential alignment in *Caulobacter crescentus*

To check whether the polarized fluorescence measurements agree with previous cryo-electron microscopy results for *Caulobacter crescentus*, we imaged C-terminal FtsZ_{Cc}-YFP of *C. crescentus* (courtesy of L. Shapiro Lab) from the side using the same setup and imaging procedures. After correction for the intrinsic polarization of the cell body, the curve shows a pronounced maximum at $\alpha = 90°$ (Fig. S9). Using the same fitting procedure, we find that only the circumferential organization can explain this data (Fig. S9B). This is consistent with the cryo-EM results of Ref. [11]. Thus, our measurement appears to reproduce prior results from a different technique.

2.4 Dividing versus non-dividing cell

To check whether FtsZ organization changes during cell division and septum formation, we examined the polarization signal for dividing versus non-dividing cells. Two methods were utilized. In the first method, we classify cells by the presence of a visible septum (Fig. S10, A and B). These cells show similar level of polarization anisotropy. There is no difference between cells with septum and without. Next, we synchronize cells in grown in poor nutrient conditions. The synchronization and measurement procedures are discussed in the Materials and Methods section. In side view, the polarization anisotropy results are shown in Fig. S10. Again, we find no significant difference in

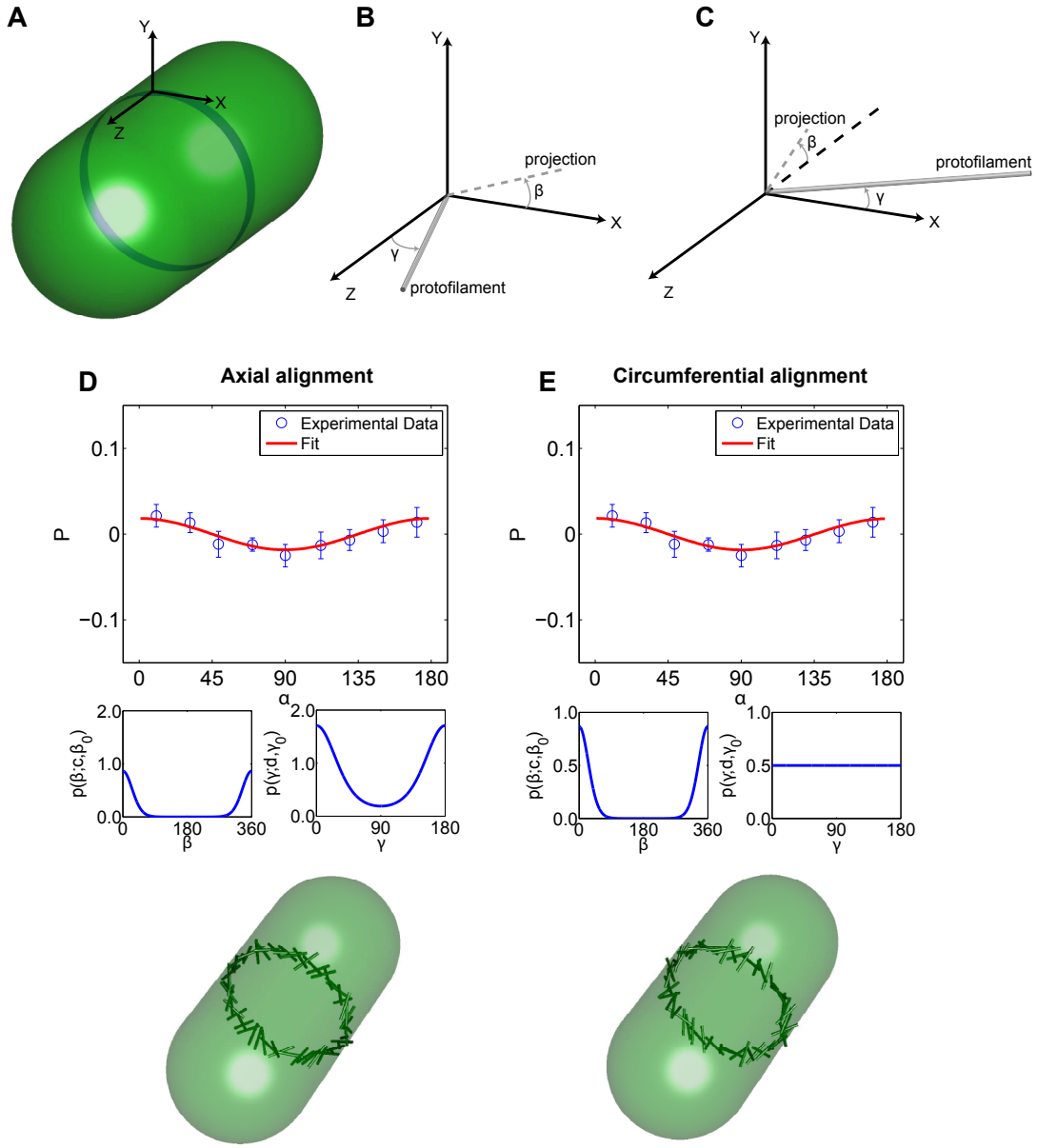

Fig. S 6: Analysis of the polarization anisotropy data from the side view for FtsZ-YFP in *E. coli*. (A) From images collected at the top of the Z-ring (slice a in the main text Figure 3), the lab coordinate frame is defined with z-axis in the cell axis direction. (B,C) Two average orientations of the FtsZ filaments are used to fit the data, the axial direction (B), and the circumferential direction (C). The filament orientations are defined by angles of γ and β. (D) Angular distribution fitted from the axial average orientation. We used the fitted distribution to generate the sample Z-ring organization which shows both axial and circumferential alignment. (E) The fitted distribution using the circumferential average orientation. The fitted distribution for γ is essentially uniform, consistent with (D). The generated Z-ring from this distribution is also essentially the same as in D, suggesting a disorganized orientation for FtsZ in the Z-ring.

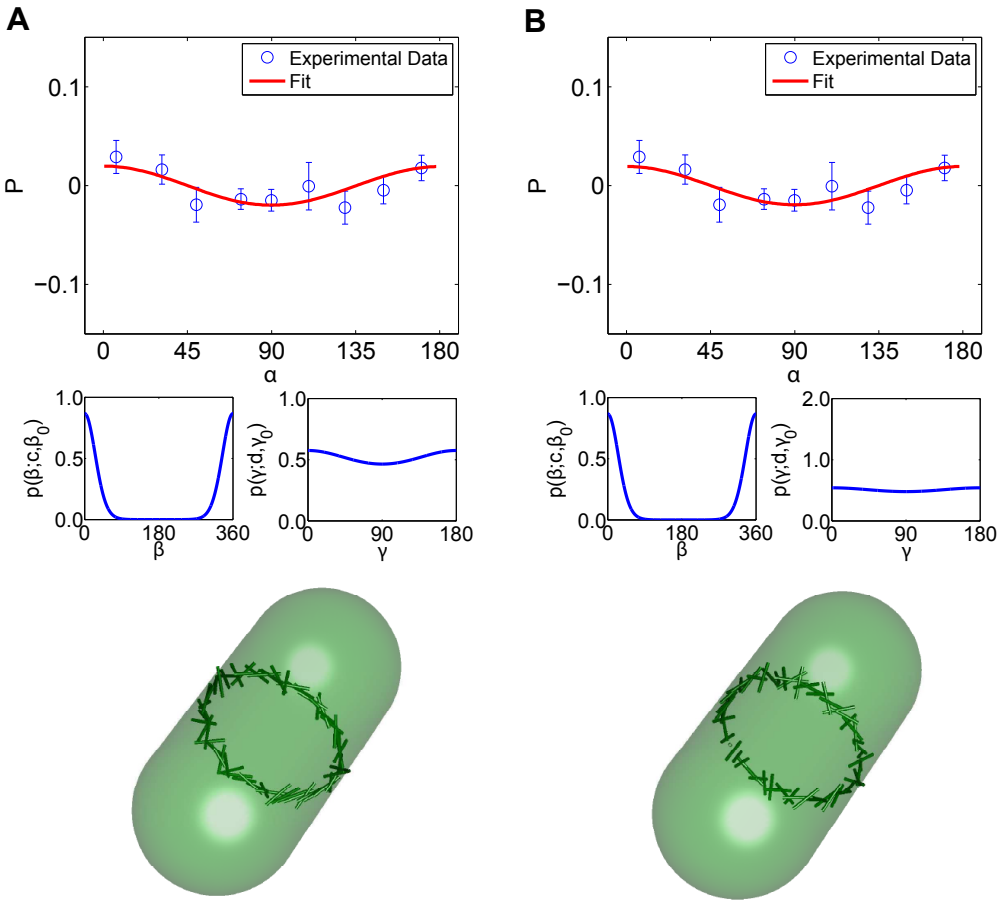

Fig. S 7: Analysis of the polarization anisotropy data from the side view for C-terminal FtsZ-GFP in *E. coli*. The results are similar to FtsZ-YFP. (A) is the fit using an average axial orientation (see Fig. S6). (B) is the fit using a circumferential average orientation. Once again, The distribution for γ is quite wide to almost uniform. The results suggest a disorganized Z-ring.

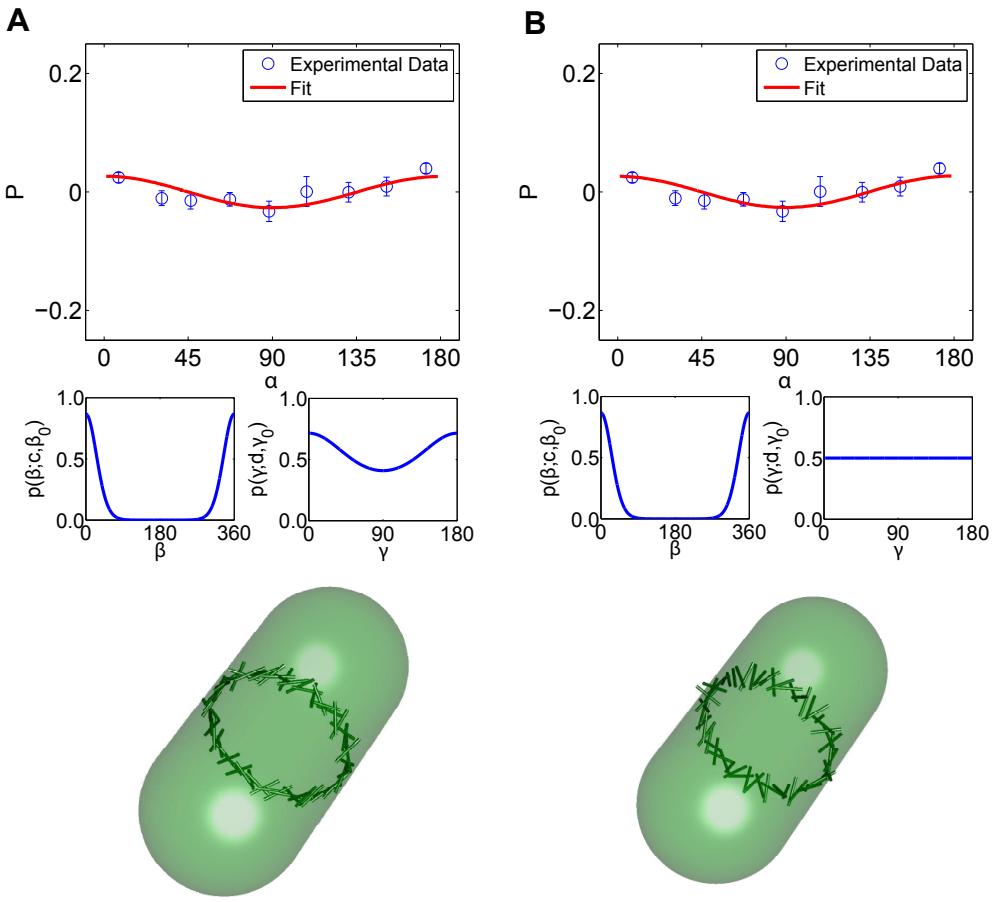

Fig. S 8: Analysis of the polarization anisotropy data from the side view for N-terminal GFP-FtsZ in *E. Coli*. (A) is the fit using an average axial orientation (see Fig. S6). (B) is the fit using a circumferential average orientation. The results are consistent with those obtained from FtsZ-YFP and FtsZ-GFP.

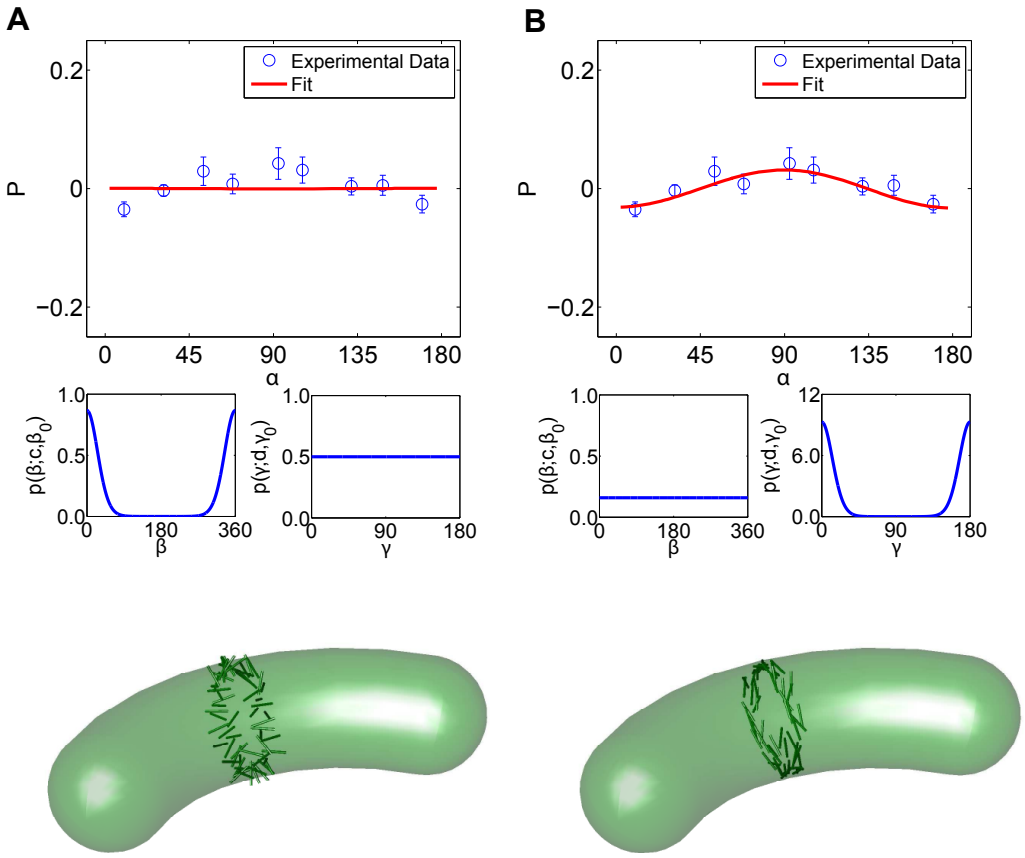

Fig. S 9: Analysis of the polarization anisotropy data from the side view for C-terminal FtsZ-YFP in *C. crescentus*. (A) is the fit using an average axial orientation (see Fig. S6). (B) is the fit using a circumferential average orientation. Now, the axial orientation cannot explain the data but the circumferential orientation fits the data well. Therefore, we conclude that FtsZ in *C. crescentus* is oriented in the circumferential direction.

FtsZ organization in dividing vs. non-dividing cells. However, the Z-ring appears to be different in poor nutrient conditions and fluorescence signal from the ring is significantly less. The polarization signal is also less pronounced in the poor nutrient condition. Therefore, these results suggest that the Z-ring is similarly disorganized before and during cell division, although the actual composition of the ring and the number of FtsZ filaments depend on nutrient level of the medium.

3 Additional Controls

3.1 Results for Septin in Yeast

To check that our results are not artifacts from the microscopy apparatus, we use the same setup to measure polarization anisotropy in a system with verified filament alignment. In *Saccharomyces cerevisiae*, the division protein septin forms a filamentous ring at the division site. It was found that during cytokinesis, the orientation of septin filaments rotate from the cell axis direction to the circumferential direction [12]. This orientation change coincides with the formation of two split division rings. Fig. S11 shows the polarization anisotropy results obtained for *S. cerevisiae* strain Cdc12-ConGFP4 (courtesy of A. Gladfelter Lab), which was used in the original experiment. Our apparatus completely reproduces the polarization change, which indicates that our measured polarization anisotropy is not an instrument artifact.

3.2 Manipulating the FtsZ-GFP Linker

As a positive control, we sought to manipulate the disordered peptide linker between FtsZ and GFP. If changes in this linker region can rotate the relative orientation of the GFP-dipole with respect to the FtsZ filament, and this rotation can be observed in live cells, then we can be confident that the GFP-dipole is an accurate reporter of the FtsZ filament orientation.

Several constructs of this type are made. These are:

- Z-Nic96linker-truncGFP (clone F10)= E. coli FtsZ (residues 1-383, full-length)-Nic96 (residues 826-831 of the 839aa protein)-GFP (residues 6-238 of the 238aa protein)
- FLAG-Z-Nic96linker-truncGFP (clone H4)
- truncZ-truncGFP (clone E2) = E. coli FtsZ (residues 1-379 of the 383aa protein)-GFP (residues 6-238 of the 238aa protein)
- FLAG-truncZ-truncGFP (clone G1)
- Z-mCherry-Z (clone 2)= E. coli FtsZ (residues 1-176 of the 383aa protein)-SGSS (linker peptide)-mCherry-SGAPG (linker peptide)-E. coli FtsZ (residues 177-383 of the 383aa protein)

Of these, only clone F10 and E2 were viable and showed significant fluorescence signal. The polarization data from these constructs are shown in Fig. S12. We see reduced polarization anisotropy and no discernible patterns. These constructs are likely disordered, which cannot report on the organization of FtsZ effectively.

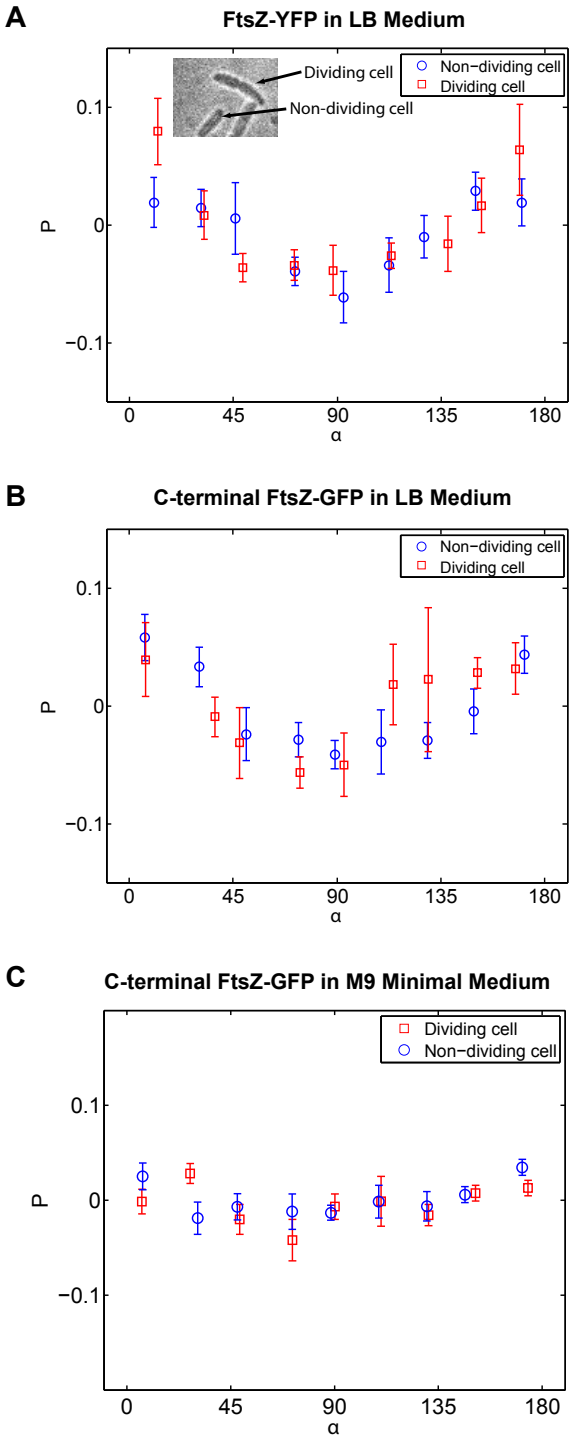

Fig. S 10: Comparison of polarization anisotropy for dividing and non-dividing *E. coli*. (A) FtsZ-YFP. (B) C-terminal FtsZ-GFP. Both results show no discernible difference between dividing and non-dividing cells, suggesting that FtsZ organization does not change during division.

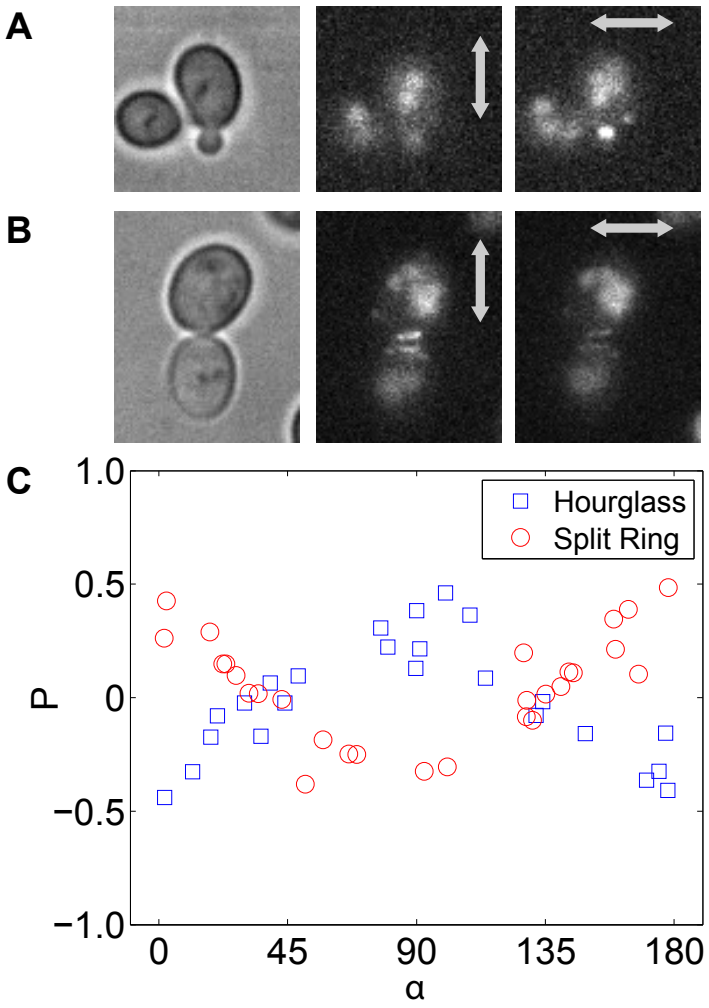

Fig. S 11: Polarization control using *S. cerevisiae*. (A) Images of Cdc12-ConGFP4 in the hourglass phase. Fluorescence images with vertical and parallel polarizer. (B) Images of Cdc12-ConGFP4 in the split ring phase. Fluorescence images with vertical and parallel polarizer. (C) Measured polarization anisotropy as a function of the angle of the cell with respect to the Lab X-axis. The complete rotation in polarization anisotropy is observed.

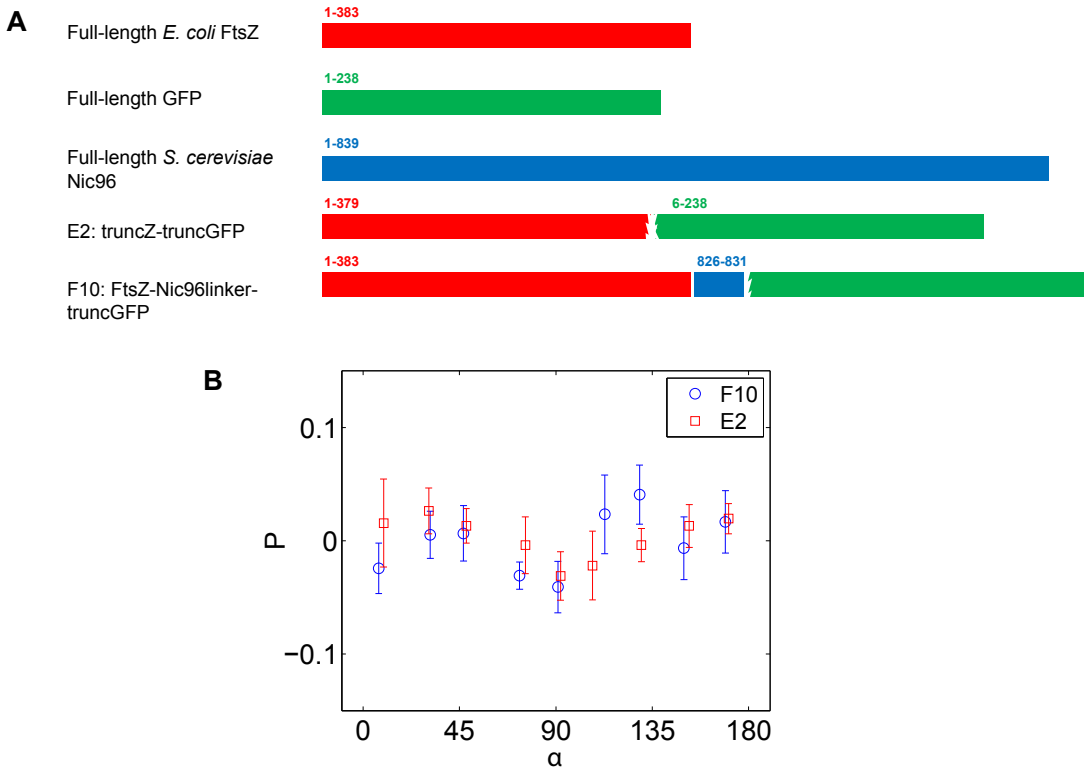

Fig. S 12: Polarization anisotropy data for Z-linker constructs F10 and E2. (A) The E2 construct is obtained by deleting several residues in the C-terminal linker between FtsZ and GFP. The F10 construct is obtained by inserting a segment of Nic96 between FtsZ and GFP. (B) The polarization data for these constructs, unfortunately, did not show discernible anisotropy.

3.3 FtsZ-ring in MinCDE Deletion Cells

To examine if the organization of the Z-ring is regulated by the MinCDE system, we also measured the orientation distribution of FtsZ-GFP in MinCDE deletion strains of *E. coli*. *E. coli* cells without MinCDE have multiple Z-ring at mid cell or near the cell poles (Fig. S13). Again, our quantitative analysis show that the organization of FtsZ filaments is disordered. This is true for the mid cell as well as polar Z-rings (Fig. S13). Results seem to suggest that Z-rings are slightly more disordered in these cells. However the difference is small. Therefore, we conclude that MinCDE is not a significant factor regulating the orientation of filaments in Z-ring.

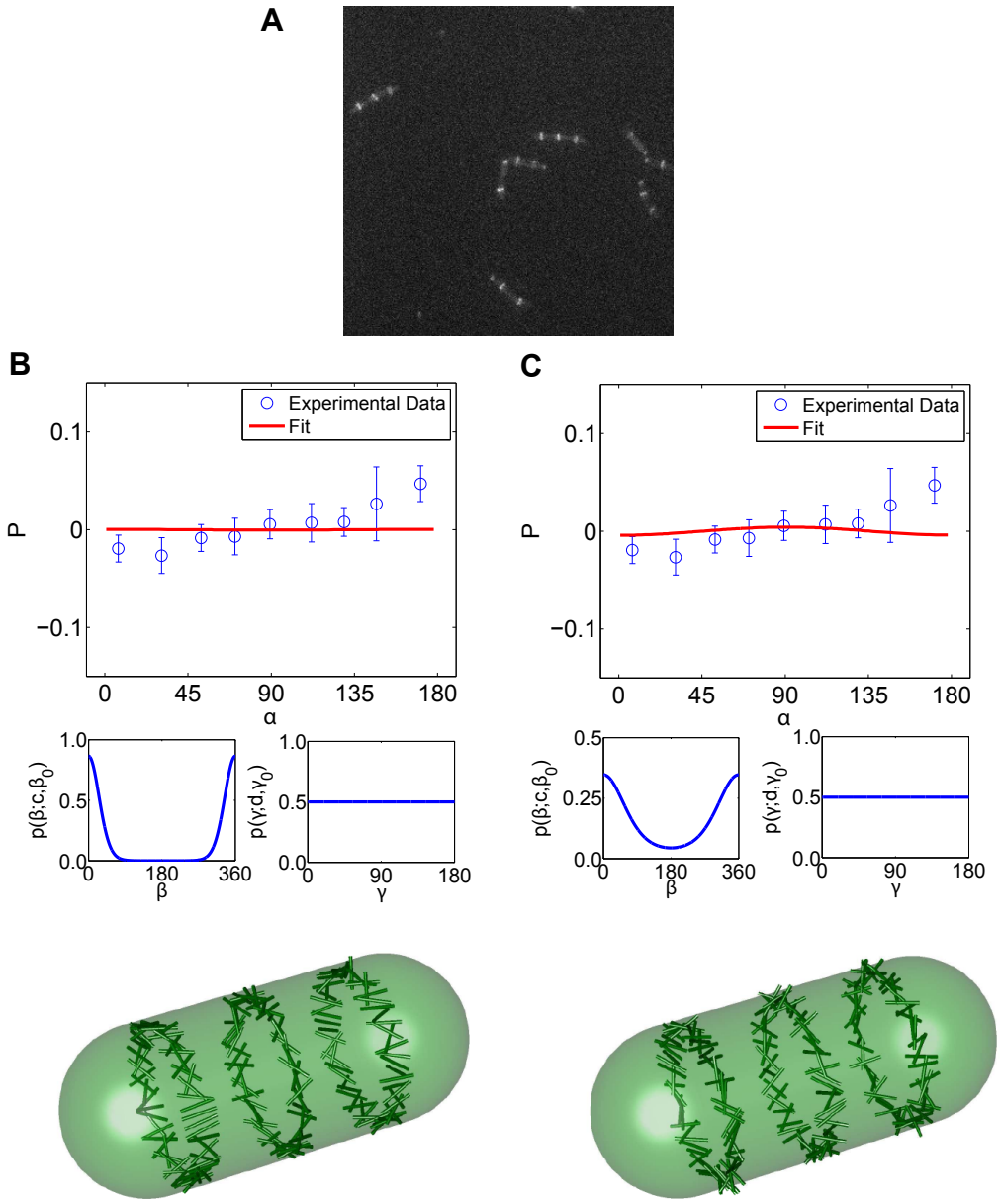

Fig. S 13: Analysis of the polarization anisotropy data from the side view for FtsZ-GFP in a MinCDE deletion strain of *E. coli*. 176 cells are included. (A) fluorescent image show that most cells have two or three Z-rings (B) Fit to the polarization anisotropy using an average axial orientation (see Fig. S6). (C) Fit to the polarization anisotropy using a circumferential average orientation. The distribution for γ is almost uniform for all Z-rings in these cells. The results suggest a disorganized Z-ring when the MinCDE system is not present.

References

[1] Ferullo DJ, Cooper DL, Moore HR, Lovett ST (2009) Cell cycle synchronization of *Escherichia coli* using the stringent response, with fluorescence labeling assays for DNA content and replication. *Methods* 48: 8-13.

[2] Kampmann M, Atkinson CE, Mattheyses AL, Simon SM (2011) Mapping the orientation of nuclear pore proteins in living cells with polarized fluorescence microscopy. *Nat. Struct. Biol.*, **18**: 643-649.

[3] Richards B, Wolf E (1959) Electromagnetic diffraction in optical systems .2. Structure of the image field in an aplanatic system. *Proc. R. Soc. London A* **253**: 358-379

[4] Desper CR, Kmura I (1967) Mathematics of the polarized fluorescence experiment. *J. Appl. Phys.* **88**: 4225-4233.

[5] Volkmer A, Subramaniam V, Birch DJS, Jovin TM (2000) One- and two-photon excited fluorescence lifetimes and anisotropy decays of Green Fluorescent Proteins. *Biophys. J.* **78**: 1589-1598.

[6] Lakowicz JR (2006) *Principles of Fluorescence Spectroscopy* (Springer Science+Business Media, LLC, New York, NY), pp. 353-382. [3rd edition]

[7] Shi, X. H., J. Basran., H. E. Seward, W. Childs, C. R. Bagshaw and S. G. Boxer. 2007. Anomalous negative fluorescence Anisotropy in yellow fluorescent protein (YFP 10C): Quantitative analysis of FRET in YFP dimers. *Biochemistry.* 46:14403-14417

[8] Ha T, Laurence TA, Chemla DS, Weiss S (1999) Polarization spectroscopy of single fluorescent molecules. *J. Phys. Chem. B* 103: 6839-6850.

[9] Anderson, D. E., F. J. Gueiros-Filho, and H. P. Erickson. (2004). Assembly dynamics of FtsZ rings in Bacillus subtilis and Escherichia coli and effects of FtsZ-regulating proteins. *J. Bacteriol.* 186:5775-5781.

[10] Geissler, B., D. Shiomi, and W. Margolin. (2007). The ftsA* gain-of-function allele of Escherichia coli and its effects on the stability and dynamics of the Z ring. *Microbiology.* 153:814825.

[11] Li Z, Trimble MJ, Brun YV, Jensen GJ (2007) The structure of FtsZ filaments in vivo suggests a force-generating role in cell division. *EMBO J.* **26**: 4694-4708.

[12] Vrabiois AM, Mitchison TJ (2006) Structural insights into yeast septin organization from polarized fluorescence microscopy. *Nature*, **443**: 466-469.